

An Approach to Solar Photovoltaic Systems Simulation Utilizing Builder Block: A Case Study of A 100 MW System

Shahad Safaa Faisal  *, Emad Talib Hashim  

Department of Energy Engineering, College of Engineering, University of Baghdad, Baghdad, Iraq

ABSTRACT

This paper offers a new design, simulation, and trying out a strategy for the Photovoltaic (PV) gadget producing 100 MW. The work explores how different irradiance and PV temperature tiers have an effect on the output power. To enhance the PV system, the proposed work utilizes the Maximum Power Point Tracking (MPPT) technique with a DC-DC boost converter and a 3-phase tie inverter. These components can improve output voltage and convert it into AC electricity for integration into the application grid. The Block Builder tool is taken into consideration a key factor of this work, which enables accurate simulation of various environmental conditions inclusive of a wide range of solar radiation and PV temperature. Consequently, the electric power generated underneath varying parameters can be exactly assessed. In this work, 4 cases are simulated to assess the performance of the proposed system. The simulation results show that the proposed design gives varying output powers based on changes in solar radiation and PV temperature, which demonstrates the adaptability of the system. In Case 4, the simulation results indicate that when increasing the solar radiation, the energy starts to increase up to 85 MW when solar radiation equals 1000 W/m^2 , which occurs at 3 seconds.

Keywords: Block builder, Output power, Photovoltaic, PV temperature, Solar radiation.

1. INTRODUCTION

The rising demand for electricity, alongside growing environmental concerns, has sparked interest in renewable energy sources. The array in the proposed model consists of interconnected solar panels that convert sunlight into electricity. There are sizes various of these arrays, ranging from small residential setups to large-scale solar farms. In the array, each solar panel comprises separate PV cells that change sunlight into power. Typically, these panels are installed on different forms such as rooftops, fixed on the ground, or melded with building structures to optimize sunlight capture. The electricity produced by the solar PV model can be presented in various places such as supplied to the electrical grid, homes, businesses, and others. The increasing global interest in harnessing renewable solar energy has garnered significant attention. Many countries have initiated projects for Photovoltaic

*Corresponding author

Peer review under the responsibility of University of Baghdad.

<https://doi.org/10.31026/j.eng.2025.01.06>



This is an open access article under the CC BY 4 license (<http://creativecommons.org/licenses/by/4.0/>).

Article received: 14/06/2024

Article revised: 21/09/2024

Article accepted: 08/10/2024

Article published: 01/01/2025



(PV) power generation, accompanied by extensive research endeavors to observe, analyze, and validate the performance of PV modules (**Kubba et al., 2008; Teyabeen and Jwaid, 2023; Deville et al., 2024**). However, practical limitations often impede the establishment of simulation designs for such research. The rise in urbanization and industrialization has heightened the demand for a further effective and dependable power design. Excess power generation during periods of surplus electricity supply leads to economic inefficiencies (**Munoz et al., 2018; Nadaleti et al., 2020; Wang, 2022**). Hence, insufficient or low power and its management may lead to power outages and possible blackouts (**Mahdavian et al., 2020; Sharma et al., 2021**). However, the discontinuous nature of the PV systems forms difficulties for engineers in terms of resolving equipment and panel issues quickly (**Chow et al., 2012**). Meanwhile, other studies have been investigated predicting the PV power generation over models such as ARIMA (**Das, 2021**), Non-linear Autoregressive Exogenous Neural Networks (**Frederiksen and Cai, 2022**), and LSTM-ARMA (**Jiang et al., 2021**). Thus, improving the capability of predicting PV power generation in advance and providing stable power can enhance the efficiency of solar energy utilization.

The current methods for predicting PV power generation still have numerous weaknesses, which are often related to solar irradiance (**Chang et al., 2021**). The electrical output is affected by various factors such as the module's electrical circuitry, the type and quality of PV cells, weather conditions, and the angle of sunlight incidence (**Islam et al., 2021**). It is worth noticing that the power generation capacity of the PV system is extremely affected by the temperature of its solar cells (**Hashim and Abbood, 2016; Al-Nimr et al., 2018**). Many studies have aimed to estimate the PV output power based on a variety of weather (**Shi et al., 2012; Jung et al., 2020; Konstantinou et al., 2021**). Accurately predicting the PV power output is vital for rapidly resolving issues with panels and equipment. Contrarily, meeting consumer power demands needs adequate power sources. Nevertheless, recent power plants have struggled to provide sufficient electricity. In this regard, fossil fuel-based power plants release significant volumes of CO₂ and other gases, raising substantial environmental problems (**Akorede et al., 2010**). This is a key contributor to global warming, resulting in higher environmental temperatures.

Regulating CO₂ and other gas emissions could potentially result in a reduction in global temperatures (**Hansen et al., 2017**). Three projected scenarios that use different energy source strategies and corresponding power conversion schemes. The first scenario, referred to as the 6 °C scenario, depicts the current trajectory without effective carbon emission controls. This path would cause significant atmospheric harm, leading to global temperature increases. As a result, polar ice caps would melt, and sea levels would rise, potentially submerging many coastal areas. Over time, the Earth's average temperature would rise by about 5.5 °C. The second scenario, the 4°C scenario, outlines a potential result where emissions are handled and energy system efficiency is improved, leading to an elevated temperature for a long time of 4 °C. The third scenario, the 2 °C scenario, proposes an ambitious strategy requiring substantial efforts to reduce emissions, aiming to limit the atmospheric temperature increase to 2 °C. This aim has to be a guiding principle for global policymaking endeavors. Accordingly, renewable energy plays a substantial role in controlling CO₂ emissions (**Hu et al., 2018**). Various sources of renewable energy exist, including wind, solar, hydro, biomass, and others (**Rahman et al., 2022**). Among these, solar energy stands out as particularly important. Solar energy systems encompass two primary types: PV and solar thermal (**Hosouli et al., 2023**). Solar thermal systems outperform PV methods concerning financial effectiveness (**Wang et al., 2019**). Moreover, the cost of PV panels was minimized, leading to enhanced performance. PV systems experience rapid



growth due to their simple setup, portability, and high application flexibility (**Wilson et al., 2020**). Moreover, the cost of PV has substantially decreased over the last few decades (**Tyagi et al., 2013**).

Recently, many studies and methods have focused on the PV modules. For instance, the work in (**Akhtar and Iqbal, 2024**), has presented a simulation study of a grid-connected three-phase PV system in Lahore using MATLAB/Simulink to investigate various scenarios. The authors have verified the accuracy of the model via three cases. In other words, they showcase the system's behavior when operating independently, during net metering with varying irradiance, and with realistic irradiance patterns. In the first case, with the grid disconnected, the PV array successfully met a 5.1 kW load demand on its own, highlighting the system's ability to operate independently and demonstrating its resilience and reliability. In the second case, the grid-connected scenario was analyzed under varying irradiance and net metering conditions. The model effectively showed power dynamics with the PV array supplying excess power to the grid during high irradiance periods and drawing power from the grid during low irradiance. This demonstrated the adaptability of the system to changing environmental conditions and the efficiency of net metering in optimizing energy use. In the third case, realistic irradiance values were used to closely replicate the day and night schedule of the site. The method precisely captured the PV system's dynamic response under these conditions which provided a realistic depiction of its performance throughout the day.

In (**Iqbal et al., 2023**), the authors proposed a design and analysis of a hybrid power system for Port Hope Simpson (PHS), Labrador, utilizing HOMER and MATLAB Simulink. The proposed system aimed to lower operating costs and address transportation challenges during winter. HOMER was used to design a new system that combines wind turbines, solar PV, and energy storage technologies with the existing three generators. While MATLAB was employed to assess the system's dynamic response. The proposed system includes 1,414 kW of PV, 1,571 kWh of battery capacity, and 1,600 kW of wind generation capacity, reducing operating costs to \$695,083 per year from the previous \$1.62 million per year. The investment is expected to have a payback period of 2.87 years and an internal rate of return (IRR) of 34.8%. By enhancing renewable resource usage and minimizing operational expenses, the hybrid power system offers long-term financial advantages to the community. In (**Patel and Bohra, 2023**), a study investigated the control and power management of the PV-wind hybrid system. The performance of the proposed system efficiently handles power across various load conditions. It explored scenarios where renewable energy sources (RES) generate either more or less power than the load demand, and where the battery capacity fluctuates at its state of charge (SOC) level. These scenarios were precisely tested through dynamic simulations in grid-connected and islanded modes. The controllers demonstrated sufficient performance in maintaining SOC levels within safe and acceptable limits. This detailed analysis will be highly beneficial for new researchers and planners in the fields of distributed generation and microgrids.

In (**Kadam et al., 2016**), the work developed a grid-connected hybrid power generation system using solar and wind energy in MATLAB/Simulink software. Furthermore, the model incorporates data on solar radiation, sunlight hours, temperature, wind speed, wind direction, and topography. By using this data, a combined solar and wind energy model can be created. In some parts of Kerala, average solar radiation is 5.68 kW/m²/day and wind speeds are 12.9 mph, with an average temperature of 28°C due to its location between the Tropic of Cancer and the equator. Independent models for PV and wind can also be simulated. In the hybrid model, components such as the solar panel, (P&O) MPPT, boost



converter, inverter, wind turbine, and PMSG generator are all connected to the grid. The PV model is tested under varying radiation and temperature environments, where the output has been observed. The presented model is simulated, and the outcomes were analyzed by utilizing MATLAB.

In **(Jayaram, 2021)**, the authors highlighted the significance of three-phase single-stage grid-connected PV systems. It primarily focuses on the operation and control of a single-stage three-phase grid-connected inverter, designed to handle various fluctuating conditions of a solar photovoltaic system. The entire system is simulated using MATLAB/Simulink software. An MPPT algorithm is employed to extract maximum power from the solar PV array. Active power is injected into the grid through this renewable energy system. The simulation results confirm the effectiveness of the proposed system.

In **(Benaissa et al., 2017)**, a group of authors detailed a grid-connected solar PV system employing a DC-DC boost converter and a DC/AC inverter (VSC) to provide electric power to the utility grid. The model represents the main components of the system, including a grid-side inverter, boost converter, and two 100 kW solar arrays. The work began with a system description, providing definitions and brief overviews of each component used in the system, examined separately. The PV cell model is straightforward, accurate, and accounts for external temperature and solar radiation. It also introduced the MPPT approach. This approach, integrated into the DC/DC converter, is employed to elevate the power output of the PV cell. Finally, the three-level DC/AC inverter (VSC) regulates the output voltage of the DC/DC converter and connects the PV array to the grid. Simulation outcomes demonstrate the impact of changing solar radiation on the power output of the PV system, as well as the control performance and dynamic behavior of the grid-connected PV method.

However, the current systems of photovoltaic (PV) still suffer from several limitations which can be listed as follows:

- Limited Simulation Designs: As mentioned in the introduction, previous studies often face practical limitations in establishing comprehensive simulation designs for PV systems under varying environmental conditions.
- Predicting PV Power Generation: Many existing models, like ARIMA, Non-linear Autoregressive Exogenous Neural Networks, and LSTM-ARMA, struggle with accurate short-term PV output forecasting due to these models relying on solar irradiance only.
- Temperature Impact: There has been limited work on quantifying the exact influence of temperature on PV performance across a wide range of conditions.

This study aims to design a Block Builder based on a specific range of solar radiation and heat. In the proposed design, there are 4 Cases of different parameters to assess its performance in various circumstances concerning variations in solar radiation and temperature. In this paper, the Block Builder is developed specifically to simulate the environmental conditions (solar radiation and temperature) affecting the PV system. This tool was programmed using a structured approach that allows for a flexible input of radiation and temperature ranges, ensuring that the system's behavior can be tested under various real-world scenarios. The Block Builder incorporates algorithms that model the nonlinear relationship between solar irradiance, temperature, and the electrical output of the PV system. It generates a dynamic dataset representing these environmental factors, which are then used to predict the performance of the PV system.

2. THE PROPOSED DESIGN

A solar energy system is currently under construction for generating electrical power via a simulation method within the MATLAB program. Besides, the simulation method will be

comprehensively outlined, accompanied by drawings and diagrams, along with explanations for each component of the system. This study aims to enhance the simulation of a 100 MW solar power plant, ensuring compliance with all electrical regulations and standards. In the proposed design, the Block Builder block was utilized to capture a specific range of solar radiation and solar PV temperature, enabling the determination of electrical power generation at various radiation and solar PV temperature levels. It also facilitates understanding the voltage behavior and resultant energy fluctuations with changes in radiation and heat. Additionally, it enables prediction of program behavior and outputs in instances of sudden decreases in solar radiation, such as when clouds suddenly obstruct sunlight to the solar panel. This Block is used to enter the variable solar radiation and temperature sinusoidal shape with a specific range as shown in **Fig. 1**. Further, all these scenarios will be investigated through program implementation using a block diagram, as illustrated in **Fig. 2**. The primary aim of the proposed design for the solar power plant is to effectively match its capacity with the consumer's load requirements. The PV power plant project encompasses various components, these components will be detailed in the subsequent subsections.

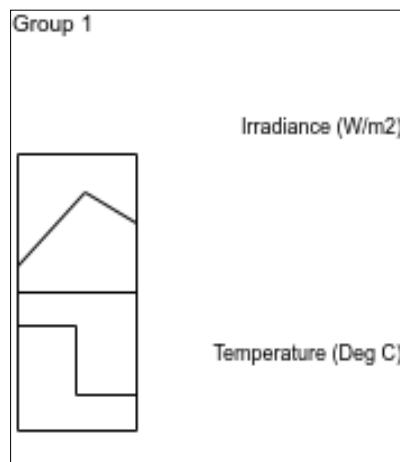


Figure 1. Signal Builder Block.

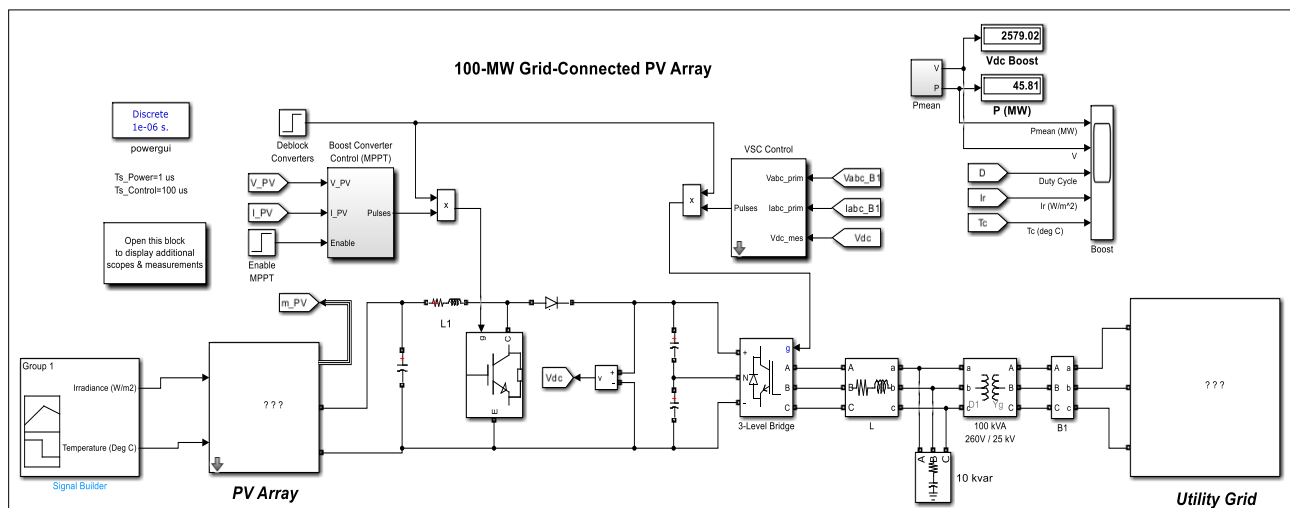


Figure 2. The proposed block diagram.

2.1 PV Array Model

In this study, the PV array model is illustrated in **Fig. 3**. Moreover, the PV array comprises strings of modules that are linked in parallel, with every string containing several linked modules. Additionally, the parameters within the PV model are adjusted to match the characteristics of four modules measured under standard test circumstances, which include an irradiance of 1000 W/m^2 and 25 C° temperature. The module of PV SunPower SPR-305-WHT type is shown in **Fig. 3**.

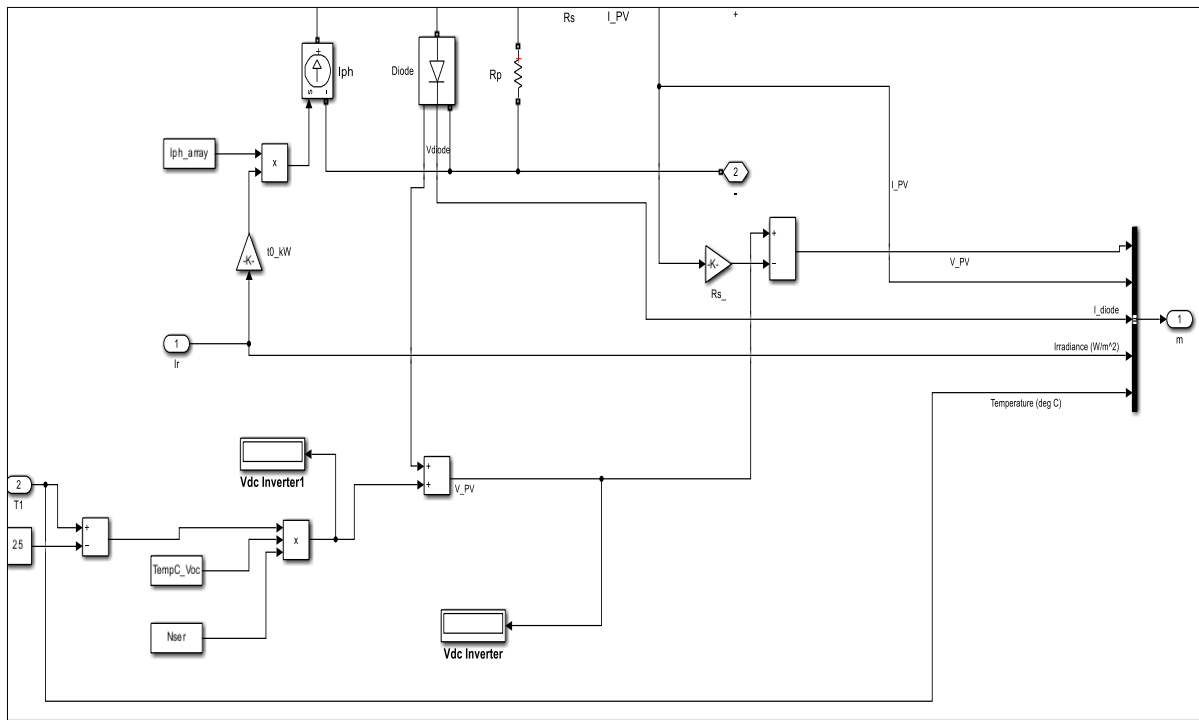


Figure 3. The model of PV array.

In the proposed method, the number of PV in parallel per string is 6600, the number of PV in series is 50, and 305 watts is the power of one PV model. Then, the output power = $6600 \times 50 \times 305 = 100650000 \text{ W} = 100.5 \text{ MW}$. **Table.1** describes the PV array model. In addition, **Fig. 4** shows a schematic diagram for a solar panel array.

Table 1. The PV array model.

| Electrical Data | | |
|--------------------------|----------------|---------------------|
| Peak power (+/5%) | Pmax | 305 W |
| Rated Voltage | V mp | 54.7 V |
| Rated Current | Imp | 5.58 A Open Circuit |
| Open Circuit Voltage | V oc | 64.2 V |
| Short Circuit Current | I sc | 5.96 A |
| Maximum System Voltage | IEC, UL | 1000 V, 600 V |
| Temperature Coefficients | | |
| | Power | -0.38%/C |
| | Voltage (V oc) | -176.6 mV/C |
| | Current (I sc) | 3.5 mA/C |
| Series Fuse Robing | | 15 A |

| | | |
|------------------------------------|---|---------------------------------|
| CEC PTC Rating | 282.1 W | |
| Mechanical Data | | |
| Solar Cells | 96 Sunpower all back contact monocrystalline | |
| Front Glass | 4.0 mm [5/32 in] tempered | |
| Junction Box | IP-65 rated with 3 bypass diodes | |
| Output Cables | 900 mm length cables / Mus-Contact connects | |
| Frame | Clear anodized aluminum alloy type 6063 | |
| Weight | 24 kg.53 bs | |
| Area | 1559*1049=1630714mm ² =1.63074 m ² | Width =1559mm Length=1046 mm |
| Tested Operating Conditions | | |
| Temperature | -40 C to +B5 C (-40 F TO + 185 F) | |
| Max load | 50 P _{sf} (2400 Pascals front and back) | |
| Impact Resistance | Hail -25 mm (1 inch) at 23 m/s (52 mph) | |



Figure 4. Schematic diagram of 330000 Solar PV connected

2.2 Insulated Gate Bipolar Transistor (IGBT)

The IGBT is a kind of energy semiconductor apparatus used in numerous applications for high-power generation. It is identified for its ability to handle low saturation voltage, quick switching, and high voltage. Furthermore, the IGBT is used together with a parallel RC snubber circuit, as illustrated in Fig. 5.

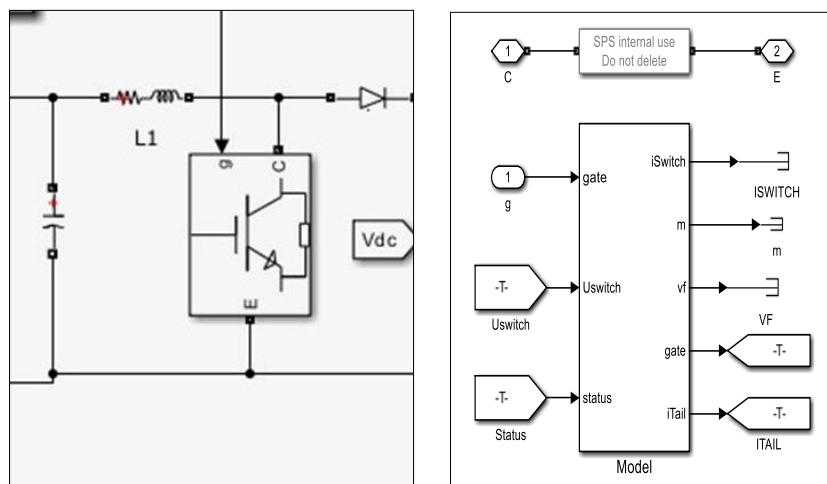


Figure 5. IGBT model and IGBT block.

The IGBT model includes inductance (L_{on}) and internal resistance (R_{on}). In most applications, L_{on} is set to zero. When the IGBT is in the off-state, it has infinite impedance. The internal resistance R_{on} is 0.001Ω , and the snubber resistance R_s is $1 \times 10^5 \Omega$.

2.3 Maximum Power Point Tracking (MPPT)

A crucial component in the proposed method is the MPPT procedure, applied in PV solar power methods to enhance the output of solar panels (Hashim and Hussien, 2018). Fig. 6 illustrates the block diagram of the MPPT utilized in this method. This technique encompasses constantly modifying the operating requirements for the PV panels to guarantee they function at their highest power point. Therefore, it maximizes the output power. This is usually accomplished using a controller or technique that scans the voltage and the panel's current, modifying the operating point to elevate power output. Additionally, the MPPT also enhances the solar power method's efficiency and increases the energy quantity gathered from the sun. The aggregate of IC and IR provides faster and greater accurate monitoring of the MPP, especially in the course of dynamic modifications in irradiance or temperature. The MPPT controller adjusts the duty cycle of the DC-DC improve converter. The improved converter steps up the voltage from the PV array to a suitable stage for grid connection. The algorithm is implemented in the Simulink model, the use of a MATLAB function block. It correctly tracks the most electricity by using continuously adjusting the running factor based on modifications in irradiance and temperature. During dynamic irradiance conditions, the set of rules is capable of maintaining premier performance For example; when irradiance ramps up or down, the MPPT ensures that the system remains at the maximum power point as long as irradiance remains constant for a brief period.

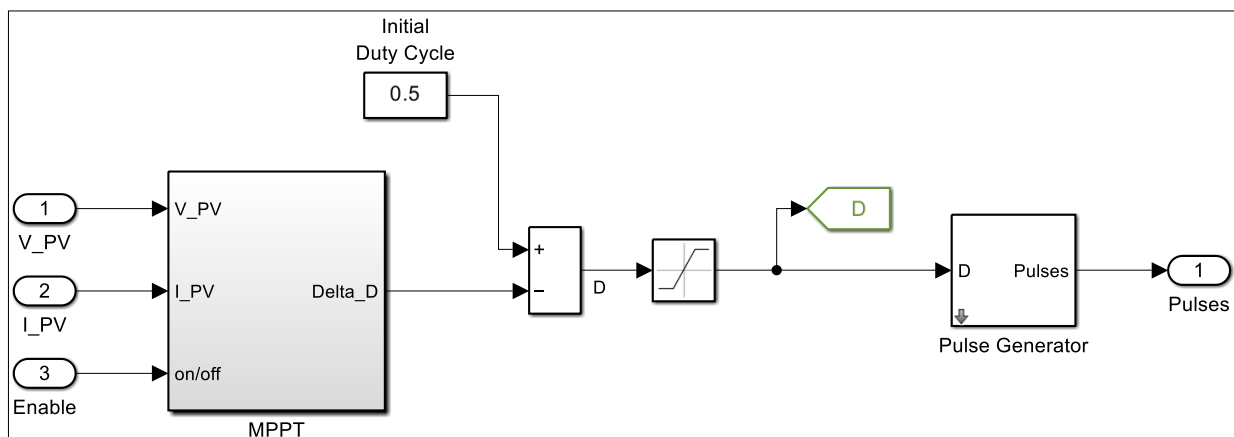


Figure 6. The MPPT block diagram.

2.3.1 Duty Cycle

In the MPPT method, the MPPT controller modifies the duty cycle of the DC-DC converter to control its operation, guaranteeing that the PV array functions at its highest power (Alwash et al., 2014). This adjustment allows the converter to modify the voltage and current levels, increasing power extraction from the PV array even as environmental conditions change. Therefore, the duty cycle is crucial in MPPT algorithms because it directly influences the performance of the DC-DC converter, enabling the PV array to maintain its MPP. Typically, the duty cycle represents the proportion of time a module is active compared to its total

operational time, usually expressed as a percentage. A duty cycle of 100% means the system is always active, while 0% means it is inactive. The duty cycle's parameters include an initial value of 0.5 and a Pulse Generator functioning at 5000 Hz frequency, as illustrated in **Fig. 7**. The duty cycle of the converter is varied according to the output of the MPPT controller, and the relationship between the input and output voltage is given by:

$$V_{out} = V_{in} / (1-D) \tag{1}$$

Where: D is the duty cycle. This combination of techniques ensures that the PV array operates at its highest efficiency under varying environmental conditions, ensuring maximum power is delivered to the grid.

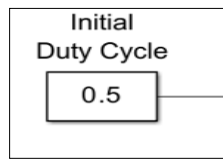


Figure 7. The Duty cycle diagram.

2.4 Voltage Source Converter Controller (VSC)

The VSC controller is a method applied in power electronics to adjust the electricity current in the topology of a three-level converter. In addition, this VSC handles the changing of semiconductor devices, such as IGBTs, to regulate the waveform of the output voltage. This is commonly used in applications like methods of renewable energy and motor drives. The controller guarantees the output voltage completes specified criteria, including voltage volume, waveform quality, and frequency while decreasing losses and preserving the stability of the system. **Fig. 8** shows the diagram which provides the parameters.

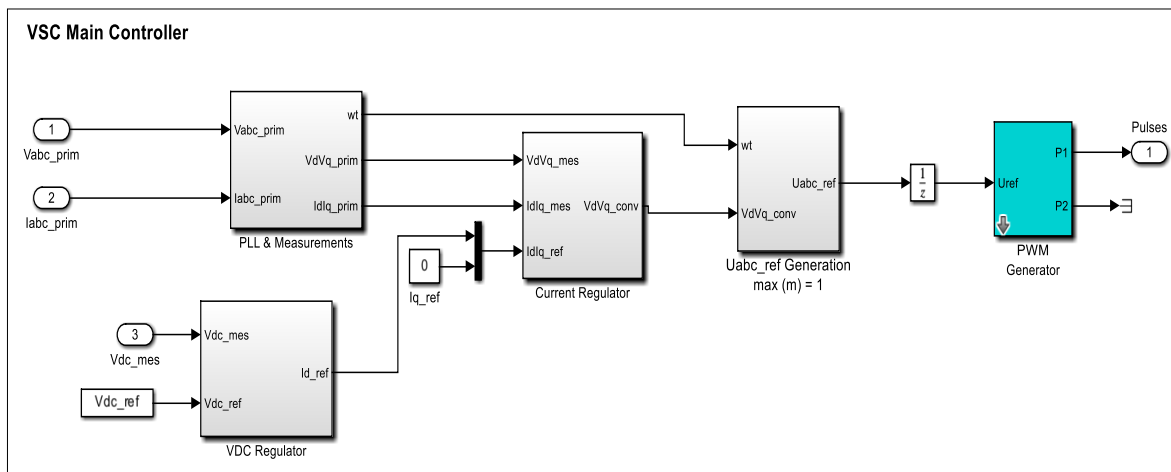


Figure 8. The diagram of the VSC.

2.5 Three-Level Bridge

A three-level bridge is a topology of power electronics converter commonly utilized in high-power applications like renewable energy, HVDC transmission, and motor drives. This bridge consists of semiconductor regulators organized in a bridge structure to manage the power flow. This system includes this bridge constructed with specifically chosen forced-

commutated power electronic devices. Further, series RC snubber circuits were linked in parallel per switch devices to enhance their performance and reliability. The parameters are detailed in **Fig. 9**. In other words, the number of arms is 3, the snubber resistance, R_S is $1 \cdot 10^6 \Omega$, and the internal resistance, R_{on} is $0.2 \cdot 10^{-3} \Omega$.

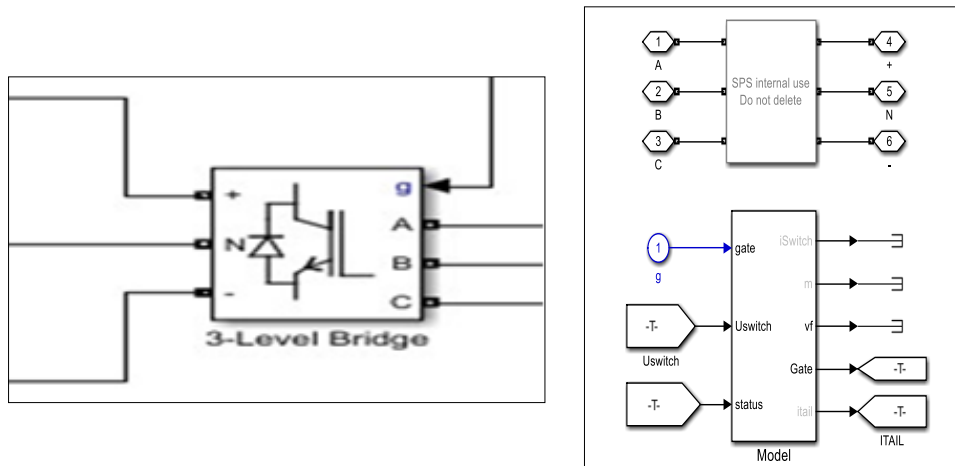


Figure 9. Block parameters for the three-level bridge.

2.6 Three-Phase Transformer

This transformer is designed for handling three-phase power. It consists of 3 groups of primary and secondary windings wound around a shared magnetic core. In addition, these transformers are commonly used in the methods of power distribution to regulate levels of voltage in networks of three-phase, either increasing or decreasing them as required. They are essential for conveying electrical power effectively and securely through extensive distances. **Fig. 10** illustrates the parameters involved in the three-phase transformer.

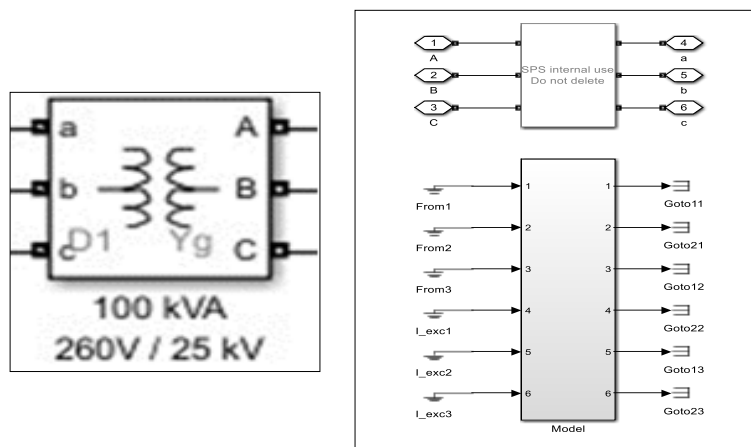


Figure 10. Three-phase transformer and block parameters.

2.7 Three-Phase Series RLC

The RLC circuit comprises Capacitors (C), Inductors (I), and Resistors (R) associated in series over a three-phase AC power source. Every circuit phase includes 1 C, 1 I, and 1 R, creating a balanced three-phase arrangement. The behavior of the series RLC circuit varies depending on the values of R, I, and C, in addition to the frequency of the AC power. It finds

applications in tasks like impedance matching, harmonic filtering, and power factor correction. Analyzing such a circuit involves examining how the resistive, inductive, and capacitive elements interact, considering frequency effects and phase angles. Further, this analysis aids in understanding distributions of voltage and current, the circuit's impedance properties, and general performance under various functioning circumstances. **Fig.11** illustrates the parameters of a three-phase series RLC branch.

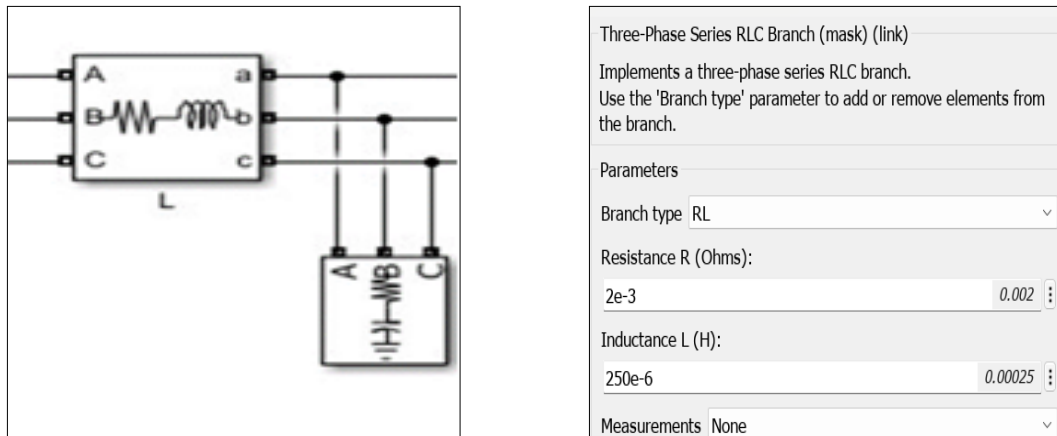


Figure 11. Three-phase series RLC block parameters.

2.8 Utility Grid

The utility grid (i.e., power grid), represents the interconnected network consisting of transmission lines, power generation facilities, transformers, substations, and distribution lines accountable for conveying electricity from power plants to end-users. It constitutes a sophisticated infrastructure system facilitating the dependable and efficient transfer of electrical power across extensive distances and diverse regions. Operating at various voltage levels along transmission lines, ranging from high voltage for long-distance transmission to lower voltage levels for local distribution, the utility grid serves homes, businesses, and industries with a consistent and dependable source of electricity. It plays a crucial role in modern society, supporting activities such as lighting, heating, cooling, manufacturing, transportation, and numerous other applications. Detailed information about the utility grid's components, including 5Km and 14Km feeders, 2MW and 30MW loads, a three-phase transformer rated at 120KV, a three-phase source also at 120KV, and a grounding transformer, can be found in **Fig.12**.

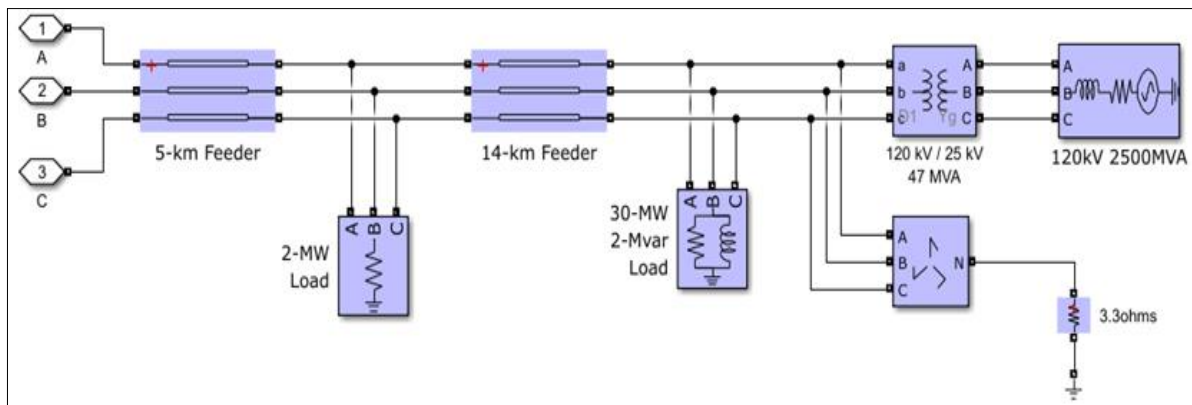


Figure 12. The Grid Utility diagram.



3. RESULTS AND DISCUSSION

The proposed design has undergone examination under various cases by using Block Builder to enter different variables. Specifically, it has been scrutinized considering different parameters, including varying solar radiations at consistent temperatures, and diverse temperature ranges at constant solar radiation levels. In addition, the proposed design using the Block Builder has been investigated based on 4 cases. Moreover, the simulation outcomes for each case will be detailed in subsequent subsections.

3.1 Case 1

In case 1, the solar radiation is introduced in the range from 250 to 1000 (W/m^2) and the temperature is a constant value at 25°C . In addition, **Fig.13** presents the simulation results of the Case 1. In the results of Case 1, we observed that the energy generated during the simulation reaches up to 10 MW initially, at a time of 0.5 seconds. It then gradually increases as solar radiation levels rise, reaching 57 MW at $400\text{W}/\text{m}^2$, 63 MW at $800\text{ W}/\text{m}^2$ m, and peaking at 82 MW at 2.5 seconds when solar radiation hits approximately $850\text{ W}/\text{m}^2$. Despite consistent solar radiation levels at 1000 and a temperature of 25°C , the energy output remains fluctuating and unstable, fluctuating between 90 and 99 MW from 3 seconds to 5.9 seconds. Regarding voltage, the highest value is reached between 0 and 3 seconds, fluctuating and remaining unstable from 3 to 5.9 seconds. At 6 seconds, the power output stabilizes at 100 MW, remaining constant until the tenth second. Voltage also stabilizes at 2800 volts for the duration of the simulation.

The output power results are evident from 0 to 0.5 seconds, initially showing a lower value due to the optimization of maximum power point tracking aimed at achieving the highest voltage. The curve illustrates the recorded values aiming for peak output power. Between 1 and 3 seconds, the power gradually increases in tandem with solar radiation, reaching 57 MW at $400\text{ W}/\text{m}^2$, then further climbing to 63 MW at $800\text{ W}/\text{m}^2$, continuing until it peaks at 82 MW at $850\text{ W}/\text{m}^2$, correlating with solar radiation levels.

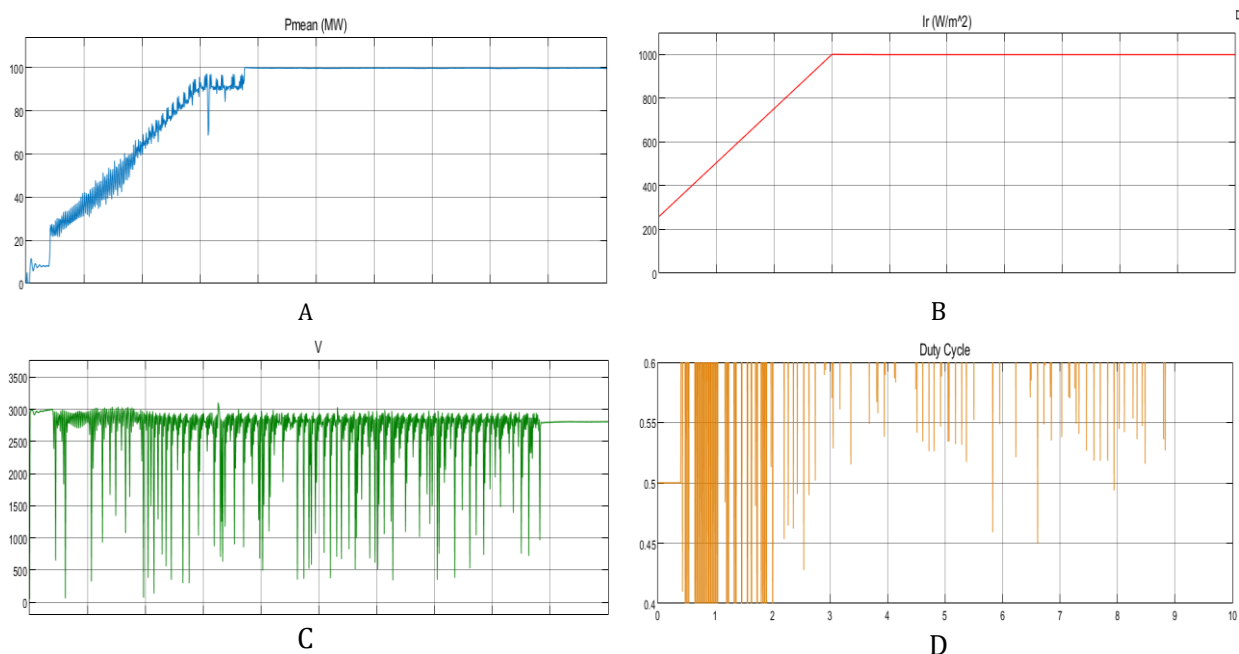


Figure 13. The simulation results of Case 1 with a constant temperature of 25°C (A. power, B. solar radiation, C. voltage, and D. duty cycle) from 0 to 10 sec.



However, during the second period, from 3 to 6 seconds, the output power fails to reach 100 MW despite standard conditions at 25°C and solar radiation at 1000 W/m², fluctuating between 90 to 97 MW due to the time taken to optimize voltage through MPPT. Finally, during the third period (6-9 seconds) and fourth period (9-10 seconds), the output power stabilizes at 100 MW until the process concludes. **Table 2** shows the overall simulation results of Case 1.

Table 2. All simulations results for Case 1.

| Time (sec) | Solar radiation G(W/m ²) | Power from measurement (MW) | Power from modeling (MW) | Error |
|------------|--------------------------------------|-----------------------------|--------------------------|-------|
| 0.1 | 280 | 28.18 | 10.91 | 0.62 |
| 0.2 | 300 | 30.19 | 7.30 | 0.75 |
| 0.5 | 400 | 40.26 | 29.88 | 0.26 |
| 1 | 500 | 50.315 | 40.51 | 0.2 |
| 2 | 760 | 76.49 | 68.35 | 0.11 |
| 3 | 1000 | 100.7 | 87.53 | 0.13 |
| 4 | 1000 | 100.7 | 88.68 | 0.12 |
| 5 | 1000 | 100.7 | 99.34 | 0.02 |
| 6 | 1000 | 100.7 | 99.34 | 0.02 |
| 7 | 1000 | 100.7 | 99.34 | 0.02 |
| 8 | 1000 | 100.7 | 99.34 | 0.02 |
| 9 | 1000 | 100.7 | 99.34 | 0.02 |
| 10 | 1000 | 100.7 | 99.34 | 0.02 |

3.2 Case 2

In Case 2, the solar radiation remains constant at a value of 1000 W/m². Meanwhile, the temperature ranges from 25 to 45 °C. Furthermore, **Fig.14** shows the simulation results of the Case 2.

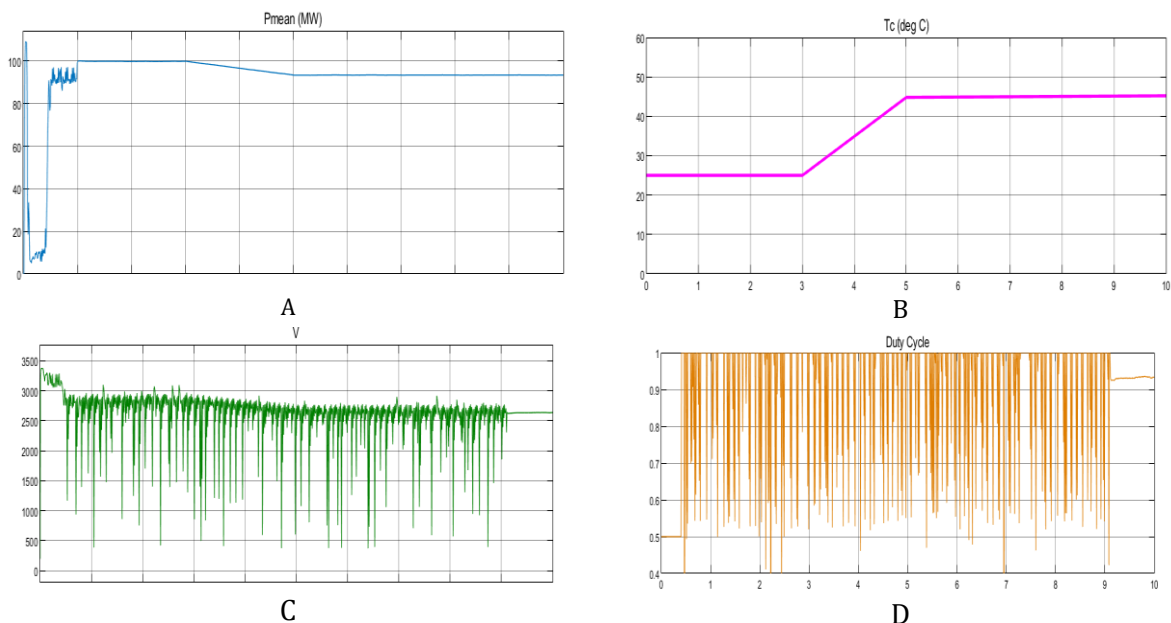


Figure 14. The simulation results of Case 2 with constant solar radiation of 1000 w/m² (A. power, B. temperature, C. voltage, and D. duty cycle) from 0 to 10 sec.



At the onset of the run period, at 0.3 seconds, the solar radiation and temperature remain at standard conditions (1000 W/m^2 , $25 \text{ }^\circ\text{C}$). Initially, the output power reaches its optimized value. However, within a few seconds (0 to 0.5 seconds), we achieve a maximum voltage value through MPPT, and the power fluctuates between 92 to 99 MW from 0.5 to 3 seconds before stabilizing at 3 seconds. Between 3 and 6 seconds, the output power begins to stabilize at 100 MW. Additionally, the temperature gradually increases, reaching $45 \text{ }^\circ\text{C}$, while the output power value decreases gradually from 92 to 90.88 MW, displaying unsteady behavior until it stabilizes at 7 seconds. The decrease in output power is attributed to the increase in ambient temperature, which reduces the efficiency of the silicon photovoltaics in the solar cell, decreasing by less than 0.3-0.5% for every $1 \text{ }^\circ\text{C}$ rise in temperature for the selected solar model, with a temperature coefficient of 0.0038 W/C° . Between 6, 9, and 10 seconds, the output power further reduces as the temperature increases, stabilizing at $45 \text{ }^\circ\text{C}$ to maintain a stable power output at 92 MW. In addition, **Table 3** illustrates all simulation results of Case 2.

Table 3. All simulations results for Case 2.

| Time (sec) | Temperature ($^\circ\text{C}$) | Power from measurement (MW) | Power from modeling (MW) | Error |
|------------|----------------------------------|-----------------------------|--------------------------|---------|
| 1 | 25 | 100.7 | 88.05 | 0.13 |
| 2 | 25 | 100.7 | 89.84 | 0.10 |
| 3 | 25 | 100.7 | 90.04 | 0.1 |
| 3.5 | 30 | 98.67 | 93.19 | 0.05 |
| 4 | 35 | 96.507 | 96.73 | 0.002 |
| 4.5 | 40 | 94.92 | 94.91 | 0.0002 |
| 5 | 45 | 92.73 | 93.11 | 0.004 |
| 6 | 45 | 92.73 | 92.81 | 0.0008 |
| 7 | 45 | 92.73 | 93.09 | 0.00388 |
| 8 | 45 | 92.73 | 93.57 | 0.006 |
| 9 | 45 | 92.73 | 93.57 | 0.009 |
| 10 | 45 | 92.73 | 93.57 | 0.009 |

3.3 Case 3

Solar radiation enters in a variable manner, characterized by sudden drops and rises. These fluctuations often coincide with cloud movements in the sky, blocking the sun's rays from reaching the solar cells. Consequently, solar radiation values decrease and then abruptly rise when the clouds dissipate. In Case 3, the temperature remained constant at $25 \text{ }^\circ\text{C}$. Besides, **Fig.15** presents the simulation results of Case 3.

In the first period (0-3 seconds), solar radiation and temperature remain at standard conditions (1000 W/m^2 , $25 \text{ }^\circ\text{C}$). The output power reaches its optimized value at 99 MW. Then, precisely at 0.5 seconds, we observed that there was a significant increase in voltage and maximum output power. During the next period (3-6 seconds), solar radiation gradually decreases to 360 W/m^2 , causing the output power to decrease to 20 MW simultaneously. At the same time, solar radiation suddenly rises to 760 W/m^2 , resulting in the output power reaching 60 MW at 4 seconds. Subsequently, solar radiation gradually decreases again to 100 W/m^2 , with power reaching 5 MW, followed by a sudden increase in solar radiation to 500 W/m^2 and power to 40 MW.

Solar radiation gradually reduces to 10 W/m^2 at 9 seconds and finally reaches 0 at 10 seconds. This case illustrates the behavior of solar radiation when clouds obstruct the



sunlight reaching the solar cells and how the system's power output becomes inefficient during such interruptions. Additionally, it demonstrates that there is no output power at 10 seconds when irradiance is zero due to the absence of solar radiation. Furthermore, Table 4 depicts all simulation results of Case 3.

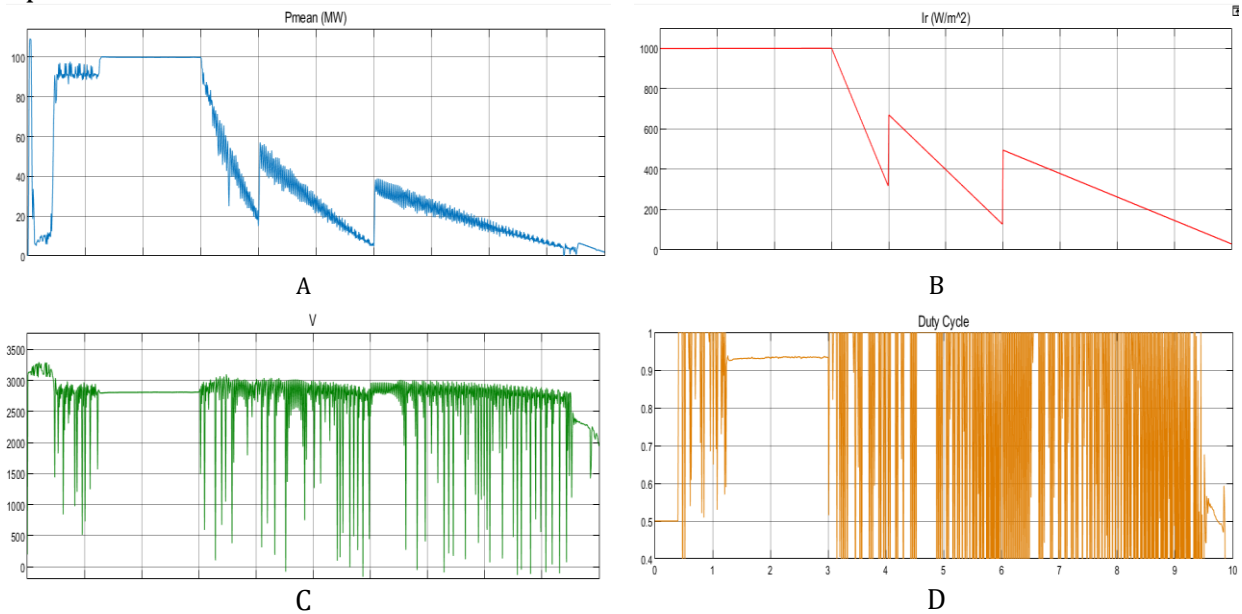


Figure 15. The simulation results of Case 3 with a constant temperature of 25 C° (A. power, B. solar radiation, C. voltage, and D. duty cycle) from 0 to 10 sec.

Table 4. All simulations results for Case 3.

| Time (sec) | Solar radiation G(W/m ²) | Power from measurement (MW) | Power from modeling (MW) | Error |
|------------|--------------------------------------|-----------------------------|--------------------------|-------|
| 1 | 1000 | 100.7 | 90.66 | 0.1 |
| 2 | 1000 | 100.7 | 97.14 | 0.04 |
| 3 | 1000 | 100.7 | 99.88 | 0.01 |
| 3.5 | 630 | 63.4 | 10.97 | 0.83 |
| 4 | 270 | 27.18 | 14.29 | 0.48 |
| 4.5 | 600 | 60.38 | 38.19 | 0.37 |
| 5 | 400 | 40.26 | 30.4 | 0.11 |
| 5.5 | 370 | 37.24 | 20.52 | 0.45 |
| 6 | 180 | 18.12 | 6.98 | 0.62 |
| 6.5 | 480 | 48.31 | 33.22 | 0.32 |
| 7 | 400 | 40.26 | 21.33 | 0.47 |
| 7.5 | 250 | 25.16 | 18.75 | 0.26 |
| 8 | 230 | 23015 | 15.59 | 0.33 |
| 9 | 170 | 17.11 | 5.28 | 0.7 |
| 10 | 0 | 0 | 0.02 | 0 |

3.4 Case 4

In Case 4, solar radiation and temperature were introduced into the system as specific parameters, with radiation values ranging between 0 and 1000 W/m², while temperature values ranged between 0 and 50 °C, as shown in Fig.16.

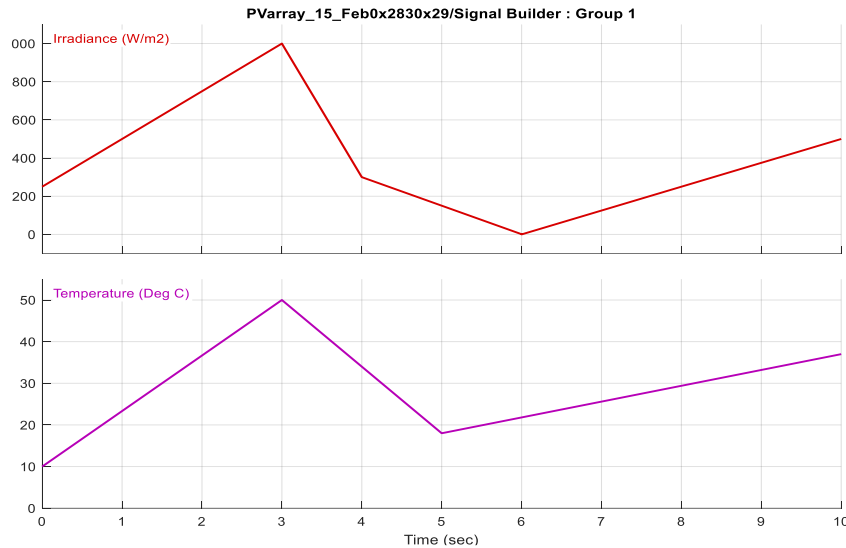


Figure 16. Variation of solar radiation with variation ambient temperature.

These values of solar radiation and temperature were selected according to readings obtained throughout the year from the Ministry of Science and Technology, Iraq. Besides, Fig.17 shows the simulation results of Case 4. In Case 4, we observed through the implementation of the second Simulink that the energy value in the initial period (0-0.3 seconds) ranges from 0 to 20 MW, as the solar radiation value is 200 W/m². This period is chosen to enable MPPT and achieve the highest voltage, thus maximizing power output, as previously mentioned. After 0.3 seconds, the energy stabilizes at 20 MW. Subsequently, with increasing solar radiation, the energy begins to rise, reaching 85 MW when solar radiation equals 1000 W/m², which occurs at 3 seconds.

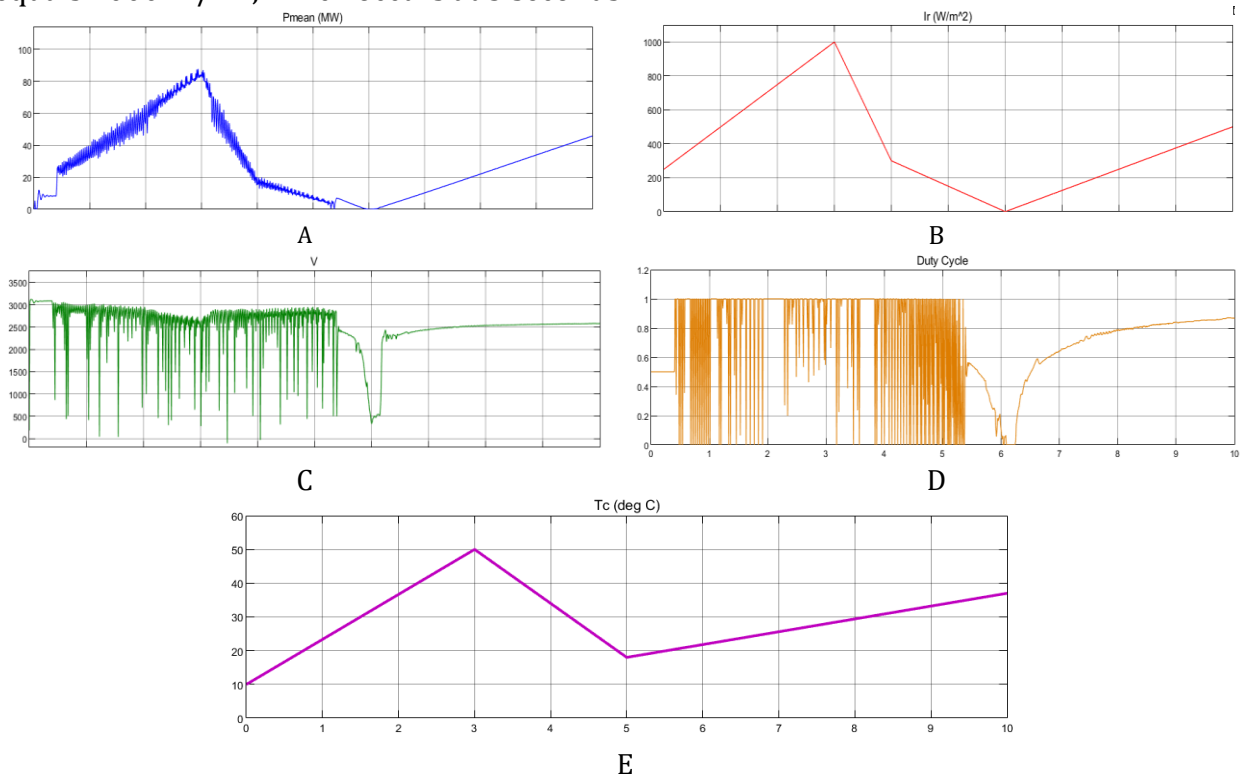


Figure 17. The simulation results of Case 4 (A. power, B. solar radiation, C. voltage, D. duty cycle, and E. temperature) from 0 to 10 sec.



However, it's noted that the energy value is less than the expected 100 MW, despite the solar radiation reaching its maximum value of 1000 W/m^2 . This is due to the effect of heat from another input into the system, where the temperature reaches 50°C . This highlights the impact of high temperatures on the performance of photovoltaic cells, reducing their effectiveness. As solar radiation decreases to 0 W/m^2 , the energy value also drops to 0 MW, as there is no energy produced in the absence of solar radiation. In addition, when solar radiation rises to 200 W/m^2 and the temperature is 30°C , the expected power output of 200 MW is achieved, as the high temperature does not affect the performance of the solar cell. By the time 10 seconds is reached, the power output is at 50 MW, with solar radiation at 500 W/m^2 and a temperature of 37°C . All simulation results of Case 4 are presented in **Table 5**.

Table 5. All simulations results for Case 4.

| Time (sec) | Solar radiation $\text{G(W/m}^2\text{)}$ | Temperature ($^\circ\text{C}$) | Power from measurement (MW) | Power from modeling (MW) | Error |
|------------|--|----------------------------------|-----------------------------|--------------------------|-------|
| 1 | 500 | 10 | 53.20 | 32.26 | 0.4 |
| 2 | 760 | 37 | 72.097 | 53.41 | 0.27 |
| 3 | 1000 | 50 | 91.09 | 83.06 | 0.09 |
| 4 | 270 | 35 | 26.13 | 19.98 | 0.24 |
| 5 | 180 | 19 | 18.53 | 5.58 | 0.7 |
| 6 | 0 | 22 | 0 | 0.02 | 0 |
| 7 | 170 | 28 | 16.91 | 10.29 | 0.4 |
| 8 | 230 | 30 | 22.72 | 22.08 | 0.03 |
| 9 | 395 | 33 | 38.49 | 33.97 | 0.12 |
| 10 | 510 | 38 | 48.78 | 45.81 | 0.06 |

The results clearly show the influence of solar radiation and temperature on the efficiency of the photovoltaic system. Increased solar radiation leads to increased power output. Meanwhile, high temperature reduces the efficiency of photovoltaic cells. The system utilizes the MPPT technology to enhance the power output, which proves its effectiveness in adjusting performance and improving system efficiency under different conditions. In general, the simulation of different cases shows that the system can adapt to the changes in various climatic conditions, but the stability depends largely on the optimal operating conditions.

4. CONCLUSIONS

The increasing request for electricity with escalating environmental crises has led to paying huge attention to renewable energy. Therefore, this paper presented an approach for designing, simulating, and testing the Photovoltaic (PV) system that can be able to generate 100 MW. The main focus of this study is investigating how changes in irradiance and temperature affect the power output of the system. The proposed work utilized the MPPT technique in conjunction with a DC-DC boost converter and a three-phase tie inverter to optimize the PV system. These components are instrumental in increasing output voltage and converting it into AC power for seamless integration into the utility grid. This work utilized the Block Builder to define specific ranges of solar radiation and temperature to facilitate the determination of electrical power generation at any given radiation and temperature level. The proposed design undergoes evaluation across four different parameter sets to assess its performance under varying solar radiation and temperature



conditions. Simulation results demonstrated that the proposed design yields diverse output powers corresponding to changes in solar radiation and temperatures that are used in each Case. In the proposed design, the maximum power output modeling values for each Case are as follows:

- **Case 1:** Maximum power output of 99.34 MW was achieved with solar radiation at 1000 W/m² and a temperature of 25°C. The increase in solar radiation from 250 W/m² to 1000 W/m² led to a rise in power output from 10 MW to 99.34MW, representing a 900% increase. In Case 1, the error ranged from 0.02 MW at 1000 W/m² (3-10 seconds) to 0.75 MW at 300 W/m².
- **Case 2:** Maximum power output of 96.73 MW was observed when the temperature reached 35°C, with solar radiation remaining constant at 1000 W/m². When the temperature increased from 25°C to 45°C at constant solar radiation of 1000 W/m², the power output decreased from 96.73MW to 93.57 MW, which means that there was a reduction of 3.16%. In Case 2, the error was as low as 0.0002 MW at 40°C.
- **Case 3:** The system's output fluctuated significantly due to variable solar radiation, peaking at 99.88MW with solar radiation at 1000 W/m² and a constant temperature of 25°C. The increase in solar radiation from 0 W/m² to 1000 W/m² led to a rise in power output from 0.02 MW to 99.88 MW, representing an increase of 99%. In Case 3, with fluctuating solar radiation, the maximum error reached 0.83 MW at 630 W/m².
- **Case 4:** The output reached 83.06 MW when solar radiation was at 1000 W/m² and the temperature was 50°C. When the solar radiation varied between 0 and 1000 W/m², and temperature ranged from 0°C to 50°C, caused the power output to range from 0 MW to 83.06 MW, an increase of 83 %, which indicates the significant impact of both factors. In Case 4, the error remained within 0.09 MW at the peak radiation level of 1000 W/m².

Credit Authorship Contribution Statement

Shahad Safaa Faisal: Writing –original draft, Validation, Methodology. Emad Talib Hashim: Review & editing, Validation, Proofreading.

Declaration of Competing Interest

The authors declare that they have no known competing financial interests or personal relationships that could have appeared to influence the work reported in this paper.

REFERENCES

- Akhtar, M. U., and Iqbal, M. T., 2024. Modeling and simulation of grid-tied Three-Phase PV system in Lahore, Pakistan. *European Journal of Electrical Engineering and Computer Science*, 8(4), pp. 23-32. <https://doi.org/10.24018/ejece.2024.8.1.603>.
- Akorede, M. F., Hizam, H., and Pouresmaeil, E., 2010. Distributed energy resources and benefits to the environment. *Renewable and sustainable energy reviews*, 14(2), pp. 724-734. <https://doi.org/10.1016/j.rser.2009.10.025>.
- Al-Nimr, M. D. A., Kiwan, S., and Sharadga, H., 2018. Simulation of a novel hybrid solar photovoltaic/wind system to maintain the cell surface temperature and to generate electricity. *International Journal of Energy Research*, 42(3), pp. 985-998. <https://doi.org/10.1002/er.3885>.



- Alwash, J. H., Hassan, T. K., and Kamel, S. W. 2014. Analysis and control of PWM buck-boost AC chopper fed single-phase capacitor run induction motor. *Journal of Engineering*, 20(06), pp. 160-178. <https://doi.org/10.31026/j.eng.2014.06.11>.
- Benaissa, O. M., Hadjeri, S., Zidi, S. A., and Benaissa, O. ,2017. Modeling and simulation of grid-connected PV generation system using Matlab/Simulink. *International Journal of Power Electronics and Drive System (IJPEDS)*, 8(1), pp. 392-401. <http://doi.org/10.11591/ijpedsv8.i1.pp392-401>.
- Chang, R., Bai, L., and Hsu, C.-H. 2021. Solar power generation prediction based on deep learning. *Sustainable energy technologies and assessments*, 47(10), 101354. <https://doi.org/10.1016/j.seta.2021.101354>.
- Chow, S. K., Lee, E. W., and Li, D. H., 2012. Short-term prediction of photovoltaic energy generation by intelligent approach. *Energy and Buildings*, 55(12), pp. 660-667. <https://doi.org/10.1016/j.enbuild.2012.08.011>.
- Das, S., 2021. Short-term forecasting of solar radiation and power output of 89.6 kW solar PV power plant. *Materials Today: Proceedings*, 39(5), pp. 1959-1969. <https://doi.org/10.1016/j.matpr.2020.08.449>.
- Deville, L., Theristis, M., King, B. H., Chambers, T. L., and Stein, J. S., 2024. Open-source photovoltaic model pipeline validation against well-characterized system data. *Progress in Photovoltaics: Research and Applications*, 32(5), pp. 291-303. <https://doi.org/10.1002/pip.3763>.
- Frederiksen, C. a. F., and Cai, Z. 2022. Novel machine learning approach for solar photovoltaic energy output forecast using extra-terrestrial solar irradiance. *Applied Energy*, 306(124), pp.118152. <https://doi.org/10.1016/j.apenergy.2021.118152>.
- Hansen, J., Sato, M., Kharecha, P., Von Schuckmann, K., Beerling, D. J., Cao, J., Marcott, S., Masson-Delmotte, V., Prather, M. J., and Rohling, E. J., 2017. Young people's burden: requirement of negative CO 2 emissions. *Earth System Dynamics*, 8(3), pp. 577-616. <https://doi.org/10.5194/esd-8-577-2017>.
- Hashim, E. T., and Abboud, A. A., 2016. Temperature effect on power drop of different photovoltaic modules. *Journal of Engineering*, 22(5), pp. 129-143. <https://doi.org/10.31026/j.eng.2016.05.09>.
- Hashim, E. T., and Hussien, S. A. M., 2018. Synchronous buck converter with Perturb and Observe Maximum Power Point Tracking Implemented on a Low-Cost Arduino microcontroller. *Journal of Engineering*, 24(2), pp. 16-33. <https://doi.org/10.31026/j.eng.2018.02.02>.
- Hosouli, S., Gomes, J., Loris, A., Pazmiño, I.-A., Naidoo, A., Lennermo, G., and Mohammadi, H., 2023. Evaluation of a solar photovoltaic thermal (PVT) system in a dairy farm in Germany. *Solar Energy Advances*, 3(2023), pp. 100035. <https://doi.org/10.1016/j.seja.2023.100035>.
- Hu, H., Xie, N., Fang, D., and Zhang, X., 2018. The role of renewable energy consumption and commercial services trade in carbon dioxide reduction: Evidence from 25 developing countries. *Applied Energy*, 211(1 February 2018), pp. 1229-1244. <https://doi.org/10.1016/j.apenergy.2017.12.019>.
- Hussain, A., Arif, S. M., and Aslam, M., 2017. Emerging renewable and sustainable energy technologies: State of the art. *Renewable and sustainable energy reviews*, 71(May 2017), pp. 12-28. <https://doi.org/10.1016/j.rser.2016.12.033>.
- Iqbal, T., Micheal, O. M., and Ogbomo, E. ,2023. Design and analysis of a hybrid power system for Port Hope Simpson, Labrador. <http://dx.doi.org/10.24018/ejece.2023.7.1.487>.



- Islam, M. A., Kassim, N. M., Alkahtani, A. A., and Amin, N., 2021. Assessing the impact of spectral irradiance on the performance of different photovoltaic technologies. *Solar Radiation-Measurement, Modeling and Forecasting Techniques for Photovoltaic Solar Energy Applications*. IntechOpen. <https://doi.org/10.5772/intechopen.96697>.
- Jayaram, K., 2021. Simulation-based three-phase single-stage grid-connected inverter using solar photovoltaics. *J. Univ. Shanghai Sci. Technol*, 23(5). <http://doi.org/10.51201/JUSST/21/05190>.
- Jiang, Y., Zheng, L., and Ding, X., 2021. Ultra-short-term prediction of photovoltaic output based on an LSTM-ARMA combined model driven by EEMD. *Journal of Renewable and Sustainable Energy*, 13(4), pp. 046103. <https://doi.org/10.1063/5.0056980>.
- Jung, Y., Jung, J., Kim, B., and Han, S., 2020. Long short-term memory recurrent neural network for modeling temporal patterns in long-term power forecasting for solar PV facilities: Case study of South Korea. *Journal of Cleaner Production*, 250(6), pp. 119476. <https://doi.org/10.1016/j.jclepro.2019.119476>.
- Kadam, P., Lahoti, G., and Shah, U. Dynamic and compact control of PV standalone system. In *2016 IEEE 1st International Conference on Power Electronics, Intelligent Control and Energy Systems (ICPEICES)*, 2016. IEEE, pp. 1-5. <https://doi.org/10.1109/ICPEICES.2016.7853454>.
- Konstantinou, M., Peratikou, S., and Charalambides, A. G., 2021. Solar photovoltaic forecasting of power output using LSTM networks. *Atmosphere*, 12(1), pp. 124. <https://doi.org/10.3390/atmos12010124>.
- Kubba, Z., Al-Shara, K., and Al-Shakarchi, E., 2008. Computer-aided design and implementation of converter circuits applied for photovoltaic System. *Journal of Engineering*, 14(04), pp. 2990-3000. <https://doi.org/10.31026/j.eng.2008.04.09>.
- Mahdavian, F., Platt, S., Wiens, M., Klein, M., and Schultmann, F., 2020. Communication blackouts in power outages: Findings from scenario exercises in Germany and France. *International Journal of Disaster Risk Reduction*, 46(June 2020), pp. 101628. <https://doi.org/10.1016/j.ijdr.2020.101628>.
- Munoz, F. D., Wogrin, S., Oren, S. S., and Hobbs, B. F., 2018. Economic inefficiencies of cost-based electricity market designs. *The Energy Journal*, 39(3), pp. 51-68. <https://doi.org/10.5547/01956574.39.3.fmun>.
- Nadaleti, W. C., Dos Santos, G. B., and Lourenço, V. A., 2020. The potential and economic viability of hydrogen production from the use of hydroelectric and wind farms surplus energy in Brazil: A national and pioneering analysis. *International Journal of Hydrogen Energy*, 45(3), pp. 1373-1384. <https://doi.org/10.1016/j.ijhydene.2019.08.199>.
- Patel, M., and Bohra, S., 2023. Power management of grid-connected PV wind hybrid system incorporated with energy storage system. *Future Energy*, 2(3), pp. 7-19. <https://doi.org/10.55670/fpll.fuen.2.3.2>.
- Rahman, A., Farrok, O., and Haque, M. M., 2022. Environmental impact of renewable energy source-based electrical power plants: Solar, wind, hydroelectric, biomass, geothermal, tidal, ocean, and osmotic. *Renewable and Sustainable Energy Reviews*, 161(June 2022), pp. 112279. <https://doi.org/10.1016/j.rser.2022.112279>.
- Sharma, N., Acharya, A., Jacob, I., Yamujala, S., Gupta, V., and Bhakar, R. 2021. Major blackouts of the decade: Underlying causes, recommendations, and arising challenges. *IEEE International Conference on Power Systems (ICPS)*, pp. 1-6. <https://doi.org/10.1109/ICPS52420.2021.9670166>.



- Shi, J., Lee, W.J., Liu, Y., Yang, Y., and Wang, P., 2012. Forecasting power output of photovoltaic systems based on weather classification and support vector machines. *IEEE Transactions on Industry Applications*, 48(3), pp. 1064-1069. <https://doi.org/10.1109/TIA.2012.2190816>.
- Teyabeen, A. A., and Jwaid, A. E., 2023. Modeling, validation, and simulation of solar photovoltaic modules. *Electrica*, 23(1). <https://doi.org/10.5152/electrica.2022.21164>.
- Tyagi, V., Rahim, N. A., Rahim, N., Jeyraj, A., and Selvaraj, L., 2013. Progress in solar PV technology: Research and achievement. *Renewable and sustainable energy reviews*, 20(April 2013), pp. 443-461. <https://doi.org/10.1016/j.rser.2012.09.028>.
- Wang, K., Herrando, M., Pantaleo, A. M., and Markides, C. N., 2019. Techno-economic assessments of hybrid photovoltaic-thermal vs. conventional solar-energy systems: Case studies in heat and power provision to sports centers. *Applied Energy*, 254(15 November 2019), pp. 113657. <https://doi.org/10.1016/j.apenergy.2019.113657>.
- Wang, X., 2022. Managing the problem of too much capital: Coal power overcapacity, migrant labor sacrifice, and structural problems in contemporary Chinese political economy. *Environment and Planning E: Nature and Space*, 5(4), pp. 1895-1918. <https://doi.org/10.1177/25148486221123418>.
- Wilson, G. M., Al-Jassim, M., Metzger, W. K., Glunz, S. W., Verlinden, P., Xiong, G., Mansfield, L. M., Stanbery, B. J., Zhu, K., and Yan, Y., 2020. The 2020 photovoltaic technologies roadmap. *Journal of Physics D: Applied Physics*, 53(49), pp. 493001. <https://doi.org/10.1088/1361-6463/ab9c6a>.

محاكاة ماتلاب لـ 100 ميغاوات من الطاقة الشمسية الكهروضوئية في ظل ظروف مناخية مختلفة

شهد صفاء فيصل*، عماد طالب هاشم

قسم هندسة الطاقة، كلية الهندسة، جامعة بغداد، بغداد، العراق

الخلاصة

قد أثار الطلب المتزايد على الكهرباء، إلى جانب المخاوف البيئية المتزايدة، الاهتمام بمصادر الطاقة المتجددة. وبناءً على ذلك، تقترح هذه الورقة تصميمًا جديدًا ومحاكاة وإجراءات اختبار لنظام كهروضوئي ينتج 100 ميغاوات. علاوة على ذلك، يركز هذا العمل على استكشاف كيفية تأثير المستويات المختلفة للإشعاع ودرجة الحرارة على الطاقة الناتجة للنظام. لتحسين النظام الكهروضوئي، فإنه يستخدم تقنية تتبع نقطة الطاقة القصوى (MPPT)، إلى جانب محول تعزيز DC-DC وعاكس ربط ثلاثي الطور. تعمل هذه المكونات على تعزيز جهد الخرج وتحويله إلى طاقة تيار متردد لدمجه في شبكة المرافق. في هذه الدراسة تم استخدام Block Builder للحصول على نطاق معين من الإشعاع الشمسي والحرارة بحيث يمكن معرفة كمية الطاقة الكهربائية المولدة عند أي قيمة للإشعاع والحرارة. هناك 4 حالات لمعلومات مختلفة مستخدمة في التصميم المقترح لتقييم أدائه في ظروف مختلفة فيما يتعلق بالتغيرات في الإشعاع الشمسي ودرجة الحرارة. أظهرت نتائج المحاكاة أن التصميم المقترح أنتج قوى إنتاجية مختلفة بناءً على تغيرات الإشعاع الشمسي ودرجات الحرارة.

الكلمات المفتاحية: إنتاج الطاقة، إشعاع شمسي، الكهروضوئية، درجة حرارة، منشئ الكتلة.